THE JOURNAL OF PHYSICAL CHEMISTRY A

Article

pubs.acs.org/JPCA

Open Access on 05/15/2015

Exciton Coupling Model for the Emergence of Second Harmonic Generation from Assemblies of Centrosymmetric Molecules

Gregory R. Snyder, Azhad U. Chowdhury, and Garth J. Simpson*

Department of Chemistry, Purdue University, West Lafayette Indiana 47907, United States

Supporting Information

ABSTRACT: A simple model is presented for interpreting the presence of substantial second harmonic generation (SHG) activity from assemblies of centrosymmetric molecular building blocks. Using butadiene as a computationally tractable centrosymmetric model system, time-dependent Hartree−Fock calculations of the nonlinear polarizability of butadiene dimer were well-described through exciton coupling arguments based on the electronic structure of the monomer and the relative orientation between the monomers within the dimer. Experimental studies of the centrosymmetric molecule 2,6-di-*tert*-butylanthraquinone suggest the formation of a combination of SHG-active and SHG-inactive crystal forms. The structure for the centrosymmetric form is known, serving as a negative control for the model, while the presence of an additional SHG-active metastable form is consistent with predictions of the model for alternative molecular packing configurations.

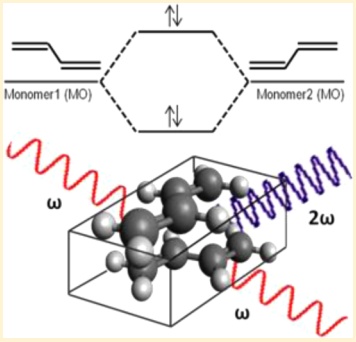

INTRODUCTION

In the design of novel organic materials for nonlinear optical applications, it initially appears irrational to consider approaches using molecular building blocks in which second harmonic generation (SHG) activity is strictly forbidden by symmetry.[1,2] However, several recent studies have reported the observation of bright SHG from appropriately arranged assemblies of centrosymmetric or nominally centrosymmetric molecules.[3−7] The rational use of purely centrosymmetric molecules as building blocks for performing frequency doubling and mixing has the potential to open up entirely new synthetic strategies for the design of organic nonlinear optical (NLO) materials. Rational design hinges first on elucidation of the dominant mechanisms driving the nonlinear optical response. However, the macromolecular mechanism underlying the emergence of SHG activity still remains a somewhat open question.

In one example using squaraines, SHG activity was observed from Langmuir−Blodgett films prepared using centrosymmetric chromophores.[3−7] The presence of SHG activity was attributed to symmetry breaking from interchromophore coupling.[8] An intermolecular charge transfer mechanism was proposed in the case of the squaraines, in which two monomers form a T-shaped dimer. However, the actual structures of the squaraine multimers are not known, given the challenges of obtaining high-resolution structures of single-monolayer organic films. While charge transfer is a sufficient condition for the presence of SHG, it is not a necessary one. It is difficult to exclude alternative chromophore dimer architectures that may produce SHG activity through coupled interactions without additional molecular-level information on the structures produced through intermolecular interactions. Within crystals of related squaraines, the monomers adopt π-stacked dimer structures,[9] or π-stacked herringbone structures[10] within the extended lattice, rather than T-shaped intermolecular structures.

In other work, vibrational sum-frequency generation (SFG) was observed from the liquid/air interface of benzene and other centrosymmetric liquids,[11,12] studied both experimentally and theoretically.[13,14] Several effects were considered to explain these observations. The observation of SFG from the benzene/air interface was first reported by Hommel and Allen, who attributed the signal to the symmetry breaking from intermolecular coupling and/or benzene dimer formation.[11] In work by Morita and co-workers, molecular dynamics calculations were coupled with interfacial hyperpolarizability and normal-mode analysis, concluding that symmetry breaking within the interfacial benzene molecules themselves was sufficient to explain the observed vibrational SFG without the need for dimerization, although bulk quadrupole contributions were also predicted to be of comparable magnitude.[13] More recently, Tahara and co-workers reported experimental results suggesting that the observed vibrational SFG from benzene may be dominated by bulk quadrupole effects.[11,12,14]

In related SHG microscopy studies of centrosymmetric carotenoids, bright SHG has recently been reported from H-aggregates of astaxanthin.[15] The astaxanthin monomers are centrosymmetric with little conformational freedom, with the known thermodynamically stable crystal form also adopting a centrosymmetric SHG-inactive lattice.[16] In addition, astaxanthin does not have a donor−acceptor−donor structure that would support partial charge transfer intermolecular inter-

Received: January 13, 2014
Revised: May 13, 2014
Published: May 15, 2014

   dx.doi.org/10.1021/jp5003935 | *J. Phys. Chem. A* 2014, 118, 4301−4308

actions. As such, the nature of the intermolecular interactions driving SHG are not trivially obvious.

Irrespective of the particular structure adopted by the dimer/multimer in the squaraines or the carotenoids, the SHG activity can likely be attributed to electronic perturbations as a consequence of intermolecular interactions. Given that the intermolecular interactions are relatively weak compared to the intramolecular interactions driving bond formation, a perturbation theoretical approach is likely to be appropriate for treating the emergence of SHG activity. Using the nonlinear optical properties of the unperturbed monomer as a starting point, the introduction of perturbations to the electronic structure can be described within the context of exciton coupling theory.[17−20]

In the present work, this simple exciton coupling approach is developed to provide a framework for describing the emergence of nonzero hyperpolarizability in noncentrosymmetric dimers of centrosymmetric molecules, serving as the foundation for predictions of larger extended clusters and aggregates. Dimer interactions form the foundation for interpreting extended multimeric intermolecular interactions, in addition to being interesting in their own right. They also have the advantage of being the smallest computationally tractable unit for describing intermolecular interactions. Quantum chemical calculations in a simple model system composed of two coupled butadiene monomers provide a framework for evaluating the strengths and limitations of the zero-order exciton coupling description. Based on the predictions of the model, crystals were prepared from centrosymmetric 2,6-di-*tert*-butylanthraquinone (TAQ) and tested experimentally by SHG microscopy.

THEORETICAL FOUNDATION

A framework for interpreting the predicted emergence of SHG activity due to coupling is proposed based on molecular orbital descriptions of the exciton states in the dimer. In centrosymmetric molecules, all vibrational and electronic transitions are exclusively one-photon- or two-photon (including Raman)-allowed, but not both. The absence of SHG can be interpreted within the context of this one-photon versus two-photon exclusivity. The molecular hyperpolarizability $\boldsymbol{\beta}^{(2)}$ tensor underlying SHG can be described by a summation over products of one-photon transition moments $\boldsymbol{\mu}$ and two-photon transition matrices $\boldsymbol{\alpha}$, provided the contributing high-energy excited states correspond to frequencies near or above the second harmonic frequency.[18,21,22]

$$\beta^{ijk}(-2\omega;\ \omega,\ \omega) = \sum_{n} S_n(2\omega)\mu_{0n}^{i}\alpha_{n0}^{jk} \tag{1}$$

The preceding equation will break down in systems exclusively exhibiting one-photon resonance enhancement or in systems not initially in the ground state, but can be considered to be an excellent approximation under most practical experimental conditions. In eq 1, $S(2\omega)$ is a complex-valued line shape function. In the case of Lorentzian line shapes, $S(2\omega)$ is given by the following equation.

$$S_n(2\omega) = \frac{1}{\hbar}\frac{1}{\omega_n - 2\omega - i\Gamma_n} \tag{2}$$

In eq 2, $\hbar\omega_n$ is the transition energy between the ground state and the nth excited state, and Γ_n is the damping constant, related to the homogeneous line width. From inspection of eq 1, the requirement that transitions be either one-photon- or two-photon-allowed clearly results in zero values for each term in the summation.

Formally, each dimer state (indicated by the subscript d) is given by summations over all of the monomer excited states (indicated by m), but with the largest contributions arising from those closest in energy.

$$\Psi_{\mathrm{d}} = \sum_{\mathrm{m}} c_{\mathrm{m}}(\psi_{\mathrm{m}}^{1} \mp \psi_{\mathrm{m}}^{2}) \tag{3}$$

So far, nothing yet has helped describe the emergence of SHG activity. If mixing only arose between the states as indicated by the solid lines in Figure 2, the $\boldsymbol{\mu}$ and $\boldsymbol{\alpha}$ terms for each exciton state in the dimer could be recovered from the sums and differences of $\boldsymbol{\mu}$ and $\boldsymbol{\alpha}$ from the corresponding transitions in the monomers. In this limit, the dimer would still exhibit no SHG, since the exciton states arising from one-photon-allowed transitions in the monomer would exhibit negligible two-photon absorption, and vice versa.

However, *minor* contributions from the other monomer excited states are also generally expected (eq 3), such that the SHG activity of the A and B states can be "turned on" through mixing in of two-photon absorption character into one-photon-allowed monomer transitions and vice versa.

EXPERIMENTAL AND COMPUTATIONAL METHODS

Electronic structure of 1,3-butadiene monomers and dimers were calculated the using GAMESS package separately. Geometry optimization calculations were used to determine the energy minimized molecular geometry, and then Avogadro software was used to orient the molecule(s) such that the z-axis was the primary axis of rotation. Configuration interaction singles (CIS) calculations were used to compute the electronic resonances of the monomer and dimer separately. Time-dependent Hartree−Fock (TDHF) calculations were used to compute first hyperpolarizability tensor elements on both the monomer and the dimer at 430, 450, and 1000 nm, with the highest energy incident frequency being within 4 nm of the first electronic resonance calculated using CIS after frequency doubling. The dimer distance was held at 3.8 Å for all three incident frequencies. Also, at 450 nm incident frequency on the dimer, TDHF calculations were used to compute first hyperpolarizability tensor elements at dimer distances of 3.8, 6.0, 8.0, and 60 Å. All calculations used the 6-311G basis set. All TDHF calculations obtained both iterative and noniterative $\boldsymbol{\beta}$ tensor elements, which were in good agreement with each other.

TDHF was selected as it has been shown to recover and describe resonant interactions, unlike conventional HF or density functional theory (DFT).[23,24] The TDHF calculations were all performed for optical frequencies approaching resonance at the second harmonic frequency consistent with the measurements but still far enough below to avoid complications from singularities that can arise near resonance.

SHG microscopy measurements of TAQ crystals were performed using an instrument described previously.[25−28] In brief, all images were acquired with a built-in-house beam scanning SHG microscope. Beam scanning was performed with a resonant vibrating mirror (~8 kHz, EOPC) along the fast-axis scan, and a galvanometer (Cambridge) for slow-axis scanning. The 800 nm excitation wavelength by a 80 MHz Ti:sapphire pulsed laser (Spectra-Physics Mai Tai) of 100 fs pulse width was directed through the scan mirrors and focused onto the

dx.doi.org/10.1021/jp5003935 | J. Phys. Chem. A 2014, 118, 4301−4308

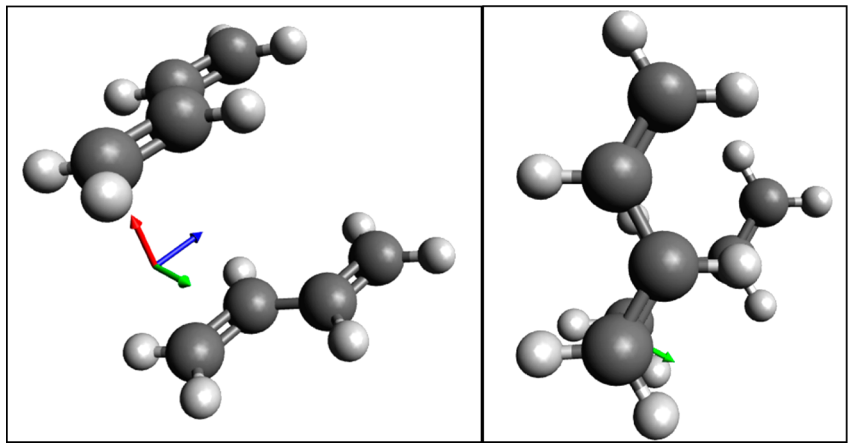

Figure 1. 1,3-Butadiene dimer used in quantum simulations, arranged so that the *z*-axis is the primary axis of rotation. The *z*-axis is blue, the *x*-axis is red, and the *y*-axis is green. The monomers are stacked on top of each other to form a "Y" shape as can be seen from the top-down view of the second image.

sample using a 10× objective of working distance 1.6 cm (Nikon, numerical aperture (N.A.) = 0.30). A 50 mW laser power was recorded at the sample. SHG signals were collected, with dichroic mirrors and narrow band-pass filters (Chroma HQ400/20 m-2p) centered around 400 nm placed prior to the photomultiplier tube detectors (Burke, XP 2920PC). An in-house-written MATLAB code was used to digitize each synchronous laser pulse with strict timing, to control the scanning mirrors and to communicate with the data acquisition electronics. Laser transmittance images were made by recording the intensity of the incident fundamental beam using a photodiode. Laser transmitted and SHG images were rendered and analyzed with the ImageJ package.

RESULTS AND DISCUSSION

Case Study 1: Butatiene Dimer. Before considering the butadiene dimer, it is useful to start with a review of the electronic structure of the monomer. Butadiene conforms to the C_{2h} point group, which is centrosymmetric and SHG-inactive by symmetry. Based on quantum chemical calculations, the two lowest energy transitions correspond to a $\pi-\pi^*$ highest occupied molecular orbital–lowest unoccupied molecular orbital (HOMO–LUMO) transition of B_u symmetry, with the next highest energy transition corresponding to B_g symmetry. As required by symmetry in centrosymmetric molecules, each transition must be allowed for either one-photon or two-photon excitation, but not both. In this case, the B_u transition is one-photon-allowed and two-photon-forbidden, while the B_g state is one-photon-forbidden and two-photon-allowed. Quantum chemical calculations of the butadiene monomer confirm these expectations, even when symmetry is not rigorously imposed.

When positioned in a π-stacking configuration such as that shown in Figure 1, the symmetry of the dimer becomes C_2, with the A and B states generated from linear combinations of the monomer states. Because of the odd symmetry of the π-orbitals, the difference states are lower in energy than the sum states in π-stacked dimers, consistent with the exciton coupling diagram depicted in Figure 2.

The exciton coupling model of a dimer is fully rigorous in the limit of inclusion of all excited states in the summation. In brief, the set of excited states serves as a basis set for recovering the new states in the coupled system. Since the excited states

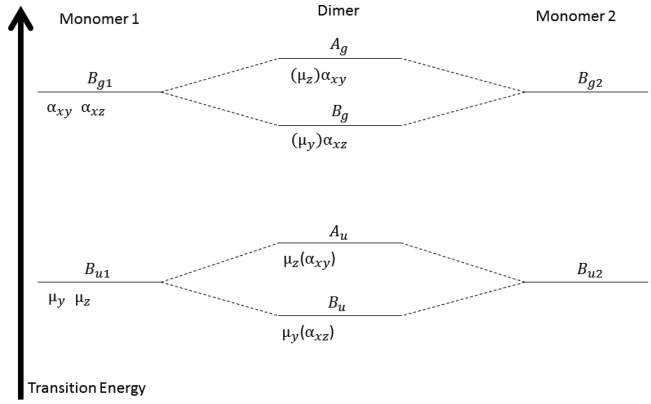

Figure 2. Exciton coupling diagram for 1,3-butadiene. Terms in parentheses represent relatively small contributions from a different dimer transition. Such overlap in molecular orbitals is allowed due to similar symmetry.

themselves are constructed from a linear combination of fundamental basis set functions, so too are the states produced from exciton coupling. In the limit of weak coupling consistent with intermolecular interactions (as opposed to covalent bond formation), each exciton state of a dimer can be reasonably described by the interactions between just one or two excited states of the monomer. However, the practical need to consider a finite number of excited state couplings can potentially introduce uncertainties in the approach. Consequently, the approach is likely to be most accurate when the coupling between monomers is relatively weak (such that only a few excited states are required to recover the exciton states) and for molecular systems with a relatively sparse population of spectrally overlapping excited states capable of participation in coupling. These are both reasonable assumptions in the present case.

Unlike the C_{2h} point group, the A and B states of the dimer can in principle each be both one-photon- and two-photon-allowed. However, in practice the core nature of the monomer transitions is carried over when describing the excited state transitions in the dimer arising from exciton coupling. Within the validity of this simple exciton coupling description, the most significant contributions to the dimer states will be produced from the sums and differences of the corresponding

dx.doi.org/10.1021/jp5003935 | J. Phys. Chem. A 2014, 118, 4301–4308

orbitals of the monomers. For example, considering just the two excited state transitions shown in Figure 2, the one-photon transition moment to the first excited B state should be recovered from the vector difference between the two monomer transition moments, resulting in a predominantly *y*-polarized transition with an oscillator strength equal to the *y*-component of the monomer multiplied by $\sqrt{2}$.

The total wave function describing the lowest excited state transition in the dimer can be written as a linear combination of both the major one-photon-allowed B_u contributions and the minor two-photon-allowed B_g contributions.

$$\Psi_B = c_{B_u}(\psi^1_{B_u} - \psi^2_{B_u}) + c_{B_g}(\psi^1_{B_g} - \psi^2_{B_g}); \quad c_{B_u} > c_{B_g} \tag{4}$$

The corresponding transition moments as well as the matrices describing two-photon absorption can be similarly produced from appropriately weighted sums and differences.

$$\mu_B = c_{B_u}(\mu^1_{B_u} - \mu^2_{B_u}) + c_{B_g}(\mu^1_{B_g} - \mu^2_{B_g}) = c_{B_u}(\mu^1_{B_u} - \mu^2_{B_u})$$
$$\alpha_B = c_{B_g}(\alpha^1_{B_g} - \alpha^2_{B_g}) \tag{5}$$

Although $|c_{B_u}| > |c_{B_g}|$, the presence of a nonzero contribution from the B_g transition provides some two-photon transition character that can drive nonzero values of the hyperpolarizability tensor $\boldsymbol{\beta}^{(2)}$. In this simplified three-state model for the monomer, the hyperpolarizability tensor for the lowest-lying B state is approximated by the following expression.

$$\beta^{ijk}_B = S_B(2\omega)\mu^i_B\alpha^{jk}_B \cong S_B(2\omega)c_{B_u}(\mu^1_{B_u} - \mu^2_{B_u})^i c_{B_g}(\alpha^1_{B_g} - \alpha^2_{B_g})^{jk}; \quad c_{B_u} > c_{B_g} \tag{6}$$

The corresponding tensor contributions for the A states are given by the summation (rather than the difference) between the monomer $\boldsymbol{\mu}$ and $\boldsymbol{\alpha}$ terms.

This model suggests several specific predictions that can be compared directly with computational and experimental results.

(1) The dominant tensor elements driving the hyperpolarizability in the dimer can be predicted based on the symmetries of the corresponding monomer states contributing to exciton coupling.

(2) In the limit of weak interchromophore coupling, the SHG activity should approach zero.

(3) The SHG activity of the dimer should be substantially enhanced close to resonance but approach zero far from resonance.

(4) Significant charge transfer is not expected for the observation of SHG activity in the dimer.

The first prediction follows directly from the analysis exemplified in eq 6. The second is clear conceptually, but potentially less so mathematically. In the limit of weak coupling, the excited state energies of an exciton pair converge to nearly degenerate values. In this limit, it becomes nearly mathematically equivalent to describe the dimer in a basis set consisting of two uncoupled monomers rather than as a coupled dimer. The key criterion has already been established for assessing whether the hyperpolarizability can be considered through the coherent summation of two uncoupled monomers, or if coupling and exciton state descriptions are required. Specifically, coupling should be considered if the energy splitting is comparable or greater than the experimental line width of the transition and can safely be neglected under conditions in which it is not.

The third prediction is closely related to the second. From inspection of eq 2, the weighting of each exciton state in the net hyperpolarizability is related to the energy difference between the exciton state and $2\hbar\omega$, where ω is the fundamental frequency. As the second harmonic frequency moves away from resonance, the contribution from each of the exciton states approaches a single constant. For example, the two exciton transition moments from the pair of B_u monomer states each contribute with approximately equal weight, such that the net result is closely approximated by the direct coherent sum of the uncoupled monomers. Correspondingly, in this limit far from resonance the perturbation from exciton coupling becomes negligible.[20,29] Since the unperturbed system of two centrosymmetric monomers is SHG-inactive, the nonresonant result should also converge to that same outcome far from resonance.

The fourth prediction is quite straightforward. Since neither of the monomers possesses a net dipole nor charge transfer character in any of the transitions, little or no charge transfer is expected in the exciton states produced from sums and differences of those same monomer states.

The predictions of the exciton coupling model were compared with the results of quantum chemical calculations of the linear and nonlinear optical properties of the butadiene monomer as a point of reference for interpreting the NLO properties of the dimer structures. CIS calculations for the monomer were performed and are summarized briefly in the Supporting Information. In brief, the lowest lying excited state corresponds to a transition of B_u symmetry, consistent with the presence of a transition moment polarized within the *xz*-plane using the coordinate system indicated in Figure 2. The next highest excited state is one-photon-forbidden, suggesting either A_g or B_g symmetry. The symmetry is tentatively assigned as B_g based on trends in the dimer detailed in following text.

The butadiene structure considered computationally was one in which just one pair of carbon atoms were coparallel and π-stacked, as shown in Figure 2. In this configuration, the butadiene dimer has C_2 symmetry. A summary of the linear optical properties of the dimer is provided in the Supporting Information.

As a simple confirmatory test, the hyperpolarizability as a function of intermolecular separation is shown in Figure 3. As

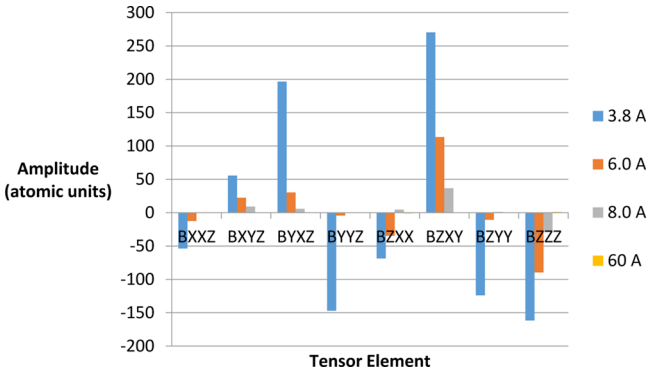

Figure 3. Calculated hyperpolarizability of 1,3-butadiene dimer at varying dimer distances. All calculations were performed at 450 nm.

one might expect, the magnitude of each hyperpolarizability tensor element uniformly decreases as the intermolecular distance is increased, asymptotically approaching a value of zero in the limit of negligible interchromophore coupling consistent with the second prediction of the exciton coupling model.

The hyperpolarizability tensor elements as a function of fundamental wavelength are summarized in Figure 4. Results

dx.doi.org/10.1021/jp5003935 | J. Phys. Chem. A 2014, 118, 4301−4308

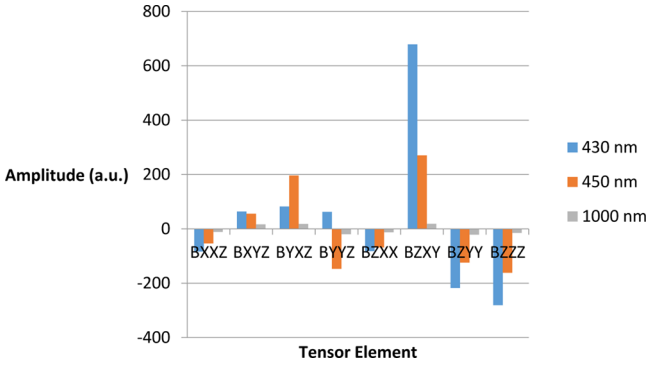

Figure 4. Calculated hyperpolarizability of the 1,3-butadiene dimer at different incident frequencies. All calculations were performed at a dimer separation of 3.8 Å.

for the frequency-dependent dimer calculations clearly demonstrate a trend in which the $\boldsymbol{\beta}$ tensor elements are rapidly reduced in magnitude as the incident wavelength is shifted further from resonance. Again, this observation is in good agreement with the predictions of the exciton coupling model.

Interestingly, the largest magnitude for the SHG activity is given in the "chiral" β_{zxy} tensor element with the largest relative enhancement close to resonance. The dominance of this contribution can be understood within the context of the exciton coupling model by considering just the two lowest excited states in the butadiene monomer. The monomer B_u (HOMO−LUMO) transition is polarized within the *yz*-plane of the chromophore and oriented largely along the long *z*-axis of the molecule. The lowest energy B exciton state in the dimer should be formed from the difference of the two monomer wave functions (given the sign difference between the p-orbitals), with symmetry dictating that it be *y*-polarized, and with a transition moment roughly $\sqrt{2}$ larger in magnitude than the monomer, in excellent agreement with the quantum chemical calculations. Similarly, the next highest excited state in the dimer should consist of the sum of the monomer wave functions, corresponding to an A state with a *z*-polarized transition moment. The major contributions to this pair of A and B states will arise from coupling primarily from just the two one-photon-allowed monomer B_u states. However, the dimer A and B states can also borrow minor contributions from the next highest two-photon-allowed excited state of B_g symmetry. For a transition of B_g symmetry, the nonzero TPA tensor elements in the monomer will be α_{xy} and α_{xz}, the first of which can contribute exclusively to A states in the dimer, and the second exclusively to B states.

Combining the nonzero elements of $\boldsymbol{\mu}$ and $\boldsymbol{\alpha}$ according to eq 1, the lowest energy dimer transition should be dominated by the β_{yxz} tensor element (nonzero μ_y and borrowed α_{xz}) and the next highest transition dominated by the β_{zxy} tensor element (large μ_z and borrowed α_{xy}). Given the larger one-photon transition moment along the long monomer *z*-axis, it is not surprising that the second excited state in the dimer

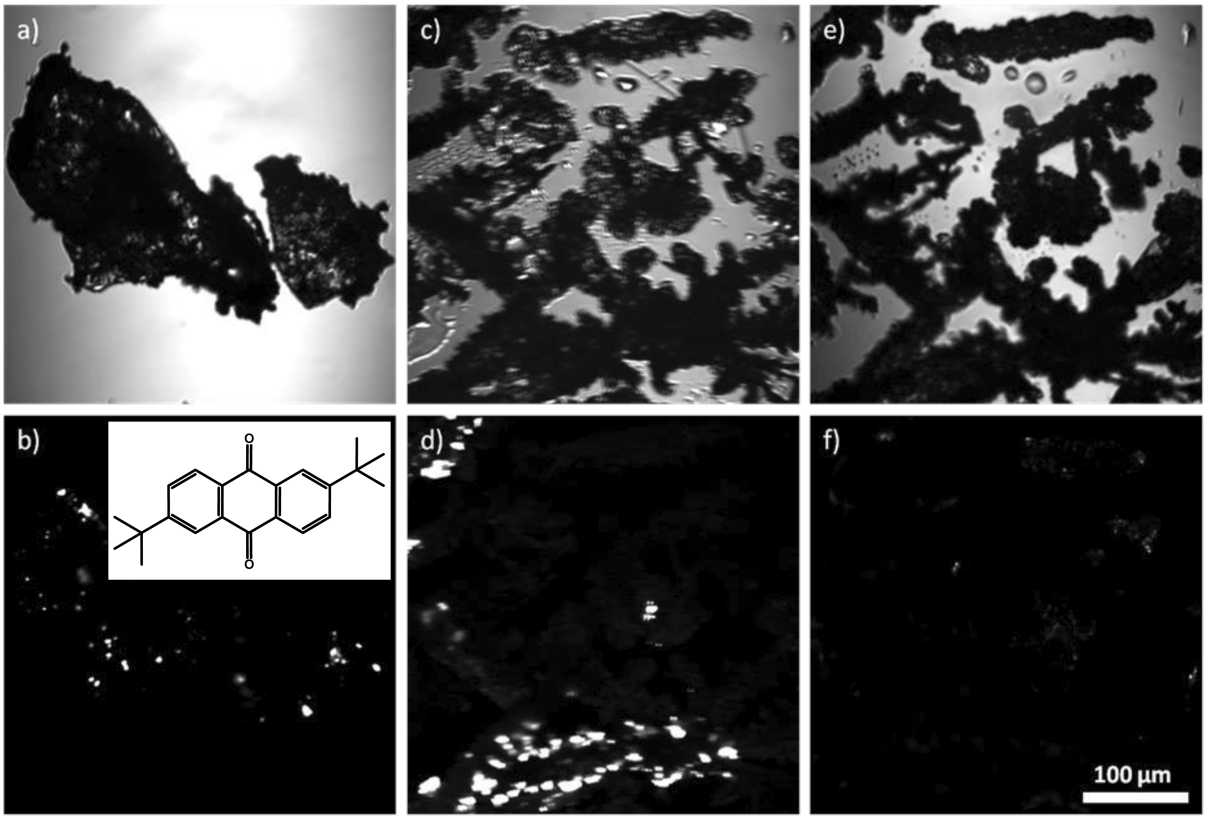

Figure 5. Laser transmitted images of TAQ from different crystallization conditions are presented (top row) along with the corresponding SHG images (bottom row). The chemical structure of TAQ is also shown in b in the inset. Panels a and b correspond to the powder as received, c and d correspond to the crystals grown by the solvent evaporation over the time course of a few minutes, and e and f are the images of the same sample following enclosure in a chamber containing high solvent vapor pressure for 3 days. The SHG images are all presented using a common intensity scale relative to a $BaTiO_3$ nanoparticle reference.

dx.doi.org/10.1021/jp5003935 | J. Phys. Chem. A 2014, 118, 4301−4308

corresponding to the β_{zxy} tensor element drives much of the NLO activity near resonance.

These combined conditions predict relatively large contributions from the "chiral" tensor elements, in reasonably good agreement with the computational results. The tensor elements β_{zyx} and β_{yxz} are larger in magnitude than all other tensor elements (at all three wavelengths considered). For example, the next most significant tensor element was β_{zzz}, presumably arising from the large μ_z from the B_u monomer transition coupled with α_{zz} contributions from the next higher excited states of B_g symmetry.

The steep sensitivity of the calculated hyperpolarizability with fundamental wavelength indicated in Figure 3 is noteworthy. This trend is consistent with the molecular orbital diagram depicted in Figure 2, assuming the "borrowing" of the one-photon and two-photon contributions goes both ways in this two excited state limit. While the lowest two excited states of the dimer yield nonzero values for β_{yxz} (nonzero μ_y and borrowed α_{xz}) and β_{zxy} (large μ_z and borrowed α_{xy}), the next highest exciton pair will similarly be driven by a large, but equal and opposite, contribution to those same tensor elements β_{yxz} (borrowed μ_y and nonzero α_{xz}) and β_{zxy} (borrowed μ_z and nonzero α_{xy}). The requirement that they sum to approximately zero in the two excited state model arises simply by the nature of the centrosymmetry of the monomers from which the dimer states were generated. Of course, additional excited states are also present and contributing, but the general sensitivity to resonance enhancement in the dimer can still be qualitatively understood within the context of this argument.

Case Study 2: 2,6-Di-*tert*-butylanthraquinone Crystals. Crystals of TAQ form a particularly useful benchmark to test the exciton coupling model. The particular set of nonzero tensor elements generated from exciton coupling depend solely on the relative orientation, and not their relative position.[16] The magnitudes of the tensor elements are affected by the degree of coupling, but not which tensor elements are nonzero. Consequently, the allowed tensor elements are arguably most easily identified by considering first structures for the TAQ dimer with different relative positions between the monomers. Based on a previously published crystal structure, TAQ forms a centrosymmetric, SHG-inactive crystal structure of $P_{\bar{1}}$ symmetry, in which every monomer is in exactly the same orientation within the lattice and each monomer is centrosymmetric.[30] Considering a dimer formed from two monomers of identical orientation, the wave functions for the sum states will simply be identical but rescaled, and all of the difference states will be zero-valued. As such, the SHG activity of the TAQ dimer and crystal is interesting to interpret within the context of the exciton coupling model. Considering a dimer composed of two monomers offset in space by not being rotated, the symmetry of the dimer is formally C_i and should result in no SHG activity.

In SHG measurements of TAQ powders as received (Figure 5), the large majority (~92.6% of the total area in the field of view) was SHG-inactive as expected based on the known crystal form. Consequently, the absence of significant SHG from the large majority of the TAQ powder is in excellent agreement with both the established bulk crystal symmetry and the exciton coupling arguments.

Since the established crystal structure for TAQ material is symmetry-forbidden for SHG,[26] it is particularly noteworthy that strong SHG is nevertheless observed from localized domains within the powdered sample. While the large majority of the TAQ powder is SHG-inactive consistent with expectations, approximately 7.4% of the total area in Figure 5a is occupied by SHG-active domains, representing a small but significant total volume fraction of the material. The SHG activities of the TAQ crystals rival those of $BaTiO_3$, used as a reference material. Recrystallization by rapid desolvation resulted in a ~10-fold increase in the integrated SHG activity of the TAQ powder per unit area, shown in Figure 5d.

Following recrystallization, the SHG-active TAQ crystals were placed in a sealed container with a saturated vapor pressure of 1,4-dioxane (the solvent used in the initial crystallization) and then reimaged after 3 days at room temperature (Figure 5e, 5f). Over this time frame, the SHG activity of the sample within the same field of view was reduced 27-fold to levels similar to those observed initially within the crystalline powder.

The observation of such a reduction in SHG from an identical region of the powder strongly suggests the absence of significant bulk-allowed quadrupolar or magnetic dipole origins for the observed SHG signals. Both higher order effects arise with comparable efficiency for both centrosymmetric and noncentrosymmetric media. As such, their contributions would be unlikely to be perturbed by the solvent-mediated recrystallization. This observation is in noteworthy contrast to vibrational SFG measurements of the benzene/air interface, in which calculations and measurements suggest quadrupole effects may be significant.[10,11] Furthermore, SHG arising from trace impurities can similarly be excluded, as they would be present in equal quantities before and after exposure to solvent vapor. In addition, the SHG intensity produced by TAQ rivals that of the noncentrosymmetric bulk dipole-allowed $BaTiO_3$ reference, which strongly suggests a bulk-allowed electric dipole origin of the observed signal.

Given the steep dependence on the preparation method, the SHG arising from the TAQ following recrystallization is attributed to the production of at least one alternative new noncentrosymmetric crystal form. In previous studies, it has been shown that rapid solvent evaporation can promote the formation of metastable polymorphs by placing crystallization under kinetic control rather than thermodynamic control.[31,32] The observed loss in SHG activity shown in Figure 5 following exposure of the crystals to solvent vapor is in good agreement with this explanation, as adsorbed solvent films can facilitate the interconversion between different crystalline solvates and/or polymorphs.[33]

Two possible mechanisms for the observed bright SHG activity within the TAQ crystals are considered. First, intermolecular interactions could be distorting TAQ to break the molecular inversion symmetry. This mechanism can be excluded by inspection of the structure of TAQ, which consists of a rigid ring with significant flexibility only in the *tert*-butyl rotation angles. It is unlikely that the relatively weak intermolecular interactions driving crystal packing will substantially distort the centrosymmetric ring structure driving the nonlinear polarizability of TAQ. It is equally unlikely that a noncentrosymmetric eclipsed configuration for the *tert*-butyl groups as opposed to the centrosymmetric staggered configuration would exhibit substantially enhanced nonlinear optical activity of the monomer. Consequently, the observation of SHG activity is attributed to intermolecular exciton coupling interactions within a noncentrosymmetric lattice.

The observation of bright SHG from TAQ crystals confirms the presence of significant intermolecular interactions within

dx.doi.org/10.1021/jp5003935 | J. Phys. Chem. A 2014, 118, 4301−4308

the lattice, but is not alone sufficient to exclusively confirm the exciton coupling model and exclude alternative mechanisms such as charge transfer. Of course, a charge transfer complex is really just a specific example of exciton coupling. Without more detailed knowledge, we can only state that the observation of SHG is consistent with the predictions of the model and that the exciton model imposes the least requirements in terms of specific structures produced than alternative hypotheses, such as charge transfer.

It is interesting that the regions of high SHG in TAQ were brighter than the $BaTiO_3$ reference materials. Given that the molecular building block is forbidden by symmetry to produce SHG, such bright signals are clear indicators of intermolecular interactions within the lattice as a key driving influence. The influence of these interactions is likely further increased through resonance enhancement. The low-lying transitions in TAQ approach energies corresponding to the twice the incident photon energy, while $BaTiO_3$ is transparent throughout the visible spectrum.

The presence of an SHG-active form for the TAQ crystals is in excellent qualitative agreement with the exciton coupling model described herein. While the packing arrangement within this new polymorph is not yet established, for the present purposes it is sufficient to note that it is clearly and strongly SHG-active, despite being produced from a centrosymmetric molecular building block.

CONCLUSION

A model based on exciton coupling theory was developed for interpreting the emergence of SHG in assemblies of centrosymmetric monomers. From the one-photon transition moments and two-photon absorption tensors within the monomer, the relative magnitudes and polarization dependences of the hyperpolarizability tensor elements describing the exciton states can be predicted based solely on the relative orientation of the monomers. The degree of energy splitting between the resulting exciton states is dependent on the coupling strength between the monomers. This approach was tested computationally using TDHF and CIS calculations on both the monomer and dimer of 1,3-butadiene, with good agreement between the predictions of the model based on the monomer optical properties and the quantum chemical calculations of the dimers. Specifically, the signs and relative magnitudes of the different $\boldsymbol{\beta}^{(2)}$ tensor elements predicted from the monomer and calculated for the dimer were in good agreement, indicating β_{zxy} as the dominant tensor contribution in the dimer at optical wavelengths. Additional experimental support for the exciton model was found in studies of TAQ crystals, in which both the SHG-active and SHG-inactive forms were found experimentally. Since TAQ is itself centrosymmetric with little conformational flexibility within the chromophore, the observation of relatively strong SHG from the metastable crystals is consistent with an exciton coupling mechanism to produce SHG-active crystalline forms.

ASSOCIATED CONTENT

Supporting Information

Table listing a detailed summary of the quantum chemical calculations for the lowest six excited states of the butadiene dimer (three excited states for the monomer) at different intermolecular distances and movie files showing the SHG and laser transmittance during crystallization of TAQ upon solvent evaporation. This material is available free of charge via the Internet at http://pubs.acs.org.

AUTHOR INFORMATION

Corresponding Author

*E-mail: gsimpson@purdue.edu.

Notes

The authors declare no competing financial interest.

ACKNOWLEDGMENTS

We gratefully acknowledge support from NIH Grant Nos. R01GM-103401 and R01GM-106484 from the NIGMS. We would also like to thank Dan Oron and Boris Rybtchinski at the Weizmann Institute of Science for their discussions and insights in the design of SHG-active crystals from centrosymmetric molecular building blocks.

REFERENCES

(1) Boyd, R. W. *Nonlinear Optics*; 3rd ed.; Academic Press: Rochester, NY, USA, 2008; pp 2−4.

(2) Shen, Y. R. *The Principles of Nonlinear Optics* (Illustrated); John Wiley & Sons: Hoboken, NJ, USA, 2003.

(3) Ashwell, G. J.; Williamson, P. C.; Bahra, G. S.; Brown, C. R. 2,4-Bis-4-(dihexadecylamino)-2-Hydroxyphenyl-Squaraine: Second-Harmonic Generation from Langmuir-Blodgett Monolayers of a Centrosymmetric Dye in Which the Chromophores Are Isolated from the Substrate. *Aust. J. Chem.* **1999**, *52*, 37−41.

(4) Honeybourne, C. L. Charge Distortion by Sparkles Can Explain Strong SHG by Centrosymmetric Squaraine Dyes. *J. Mater. Chem.* **1999**, *9*, 2241−2244.

(5) Ashwell, G. J.; Dyer, A. N.; Green, A.; Sato, N.; Sakuma, T. Monolayer Films of U-Shaped Molecules: Suppression of the Aggregation-Induced Second-Harmonic Generation of Squaraine Dyes by Guest−Host Interactions. *J. Mater. Chem.* **2000**, *10*, 2473−2476.

(6) Beverina, L.; Ruffo, R.; Patriarca, G.; De Angelis, F.; Roberto, D.; Righetto, S.; Ugo, R.; Pagani, G. A. Second Harmonic Generation in Nonsymmetrical Squaraines: Tuning of the Directional Charge Transfer Character in Highly Delocalized Dyes. *J. Mater. Chem.* **2009**, *19*, 8190.

(7) Ashwell, G. J.; Jefferies, G.; Hamilton, D. G.; Lynch, D. E.; Roberts, M. P. S.; Bahra, G. S.; Brown, C. R. Strong Second-Harmonic Generation from Centrosymmetric Dyes. *Nature* **1995**, *375*, 385−388.

(8) Honeybourne, C. L. A Mechanism for Strong SHG by Centrosymmetric Anilinosquaraine Dyes. *Adv. Mater.* **1999**, *11*, 1477−1480.

(9) Beverina, L.; Crippa, M.; Salice, P.; Ruffo, R.; Ferrante, C.; Fortunati, I.; Signorini, R.; Mari, C. M.; Bozio, R.; Facchetti, A.; et al. Indolic Squaraines as Two-Photon Absorbing Dyes in the Visible Region: X-ray Structure, Electrochemical, and Nonlinear Optical Characterization. *Chem. Mater.* **2008**, *20*, 3242−3244.

(10) Ashwell, G. J.; Bahra, G. S.; Brown, C. R.; Hamilton, D. G.; Kennard, C. H. L.; Lynch, D. E. 2,4-Bis[4-(N,N-Dibutylamino)phenyl] Squaraine: X-Ray Crystal Structure of a Centrosymmetric Dye and the Second-Order Non-Linear Optical Properties of Its Non-Centrosymmetric Langmuir?Blodgett Films. *J. Mater. Chem.* **1996**, *6*, 23.

(11) Hommel, E. L.; Allen, H. C. The Air-Liquid Interface of Benzene, Toluene, M-Xylene, and Mesitylene: A Sum Frequency, Raman, and Infrared Spectroscopic Study. *Analyst* **2003**, *128*, 750.

(12) Matsuzaki, K.; Nihonyanagi, S.; Yamaguchi, S.; Nagata, T.; Tahara, T. Vibrational Sum Frequency Generation by the Quadrupolar Mechanism at the Nonpolar Benzene/Air Interface. *J. Phys. Chem. Lett.* **2013**, *4*, 1654−1658.

(13) Kawaguchi, T.; Shiratori, K.; Henmi, Y.; Ishiyama, T.; Morita, A. Mechanisms of Sum Frequency Generation from Liquid Benzene: Symmetry Breaking at Interface and Bulk Contribution. *J. Phys. Chem. C* **2012**, *116*, 13169−13182.

(14) Rivera, C. A.; Fourkas, J. T. Reexamining the Interpretation of Vibrational Sum-Frequency Generation Spectra. *Int. Rev. Phys. Chem.* **2011**, *30*, 409−443.
(15) Tokarz, D.; Cisek, R.; Garbaczewska, M.; Sandkuijl, D.; Qiu, X.; Stewart, B.; Levine, J. D.; Fekl, U.; Barzda, V. Carotenoid Based Bio-Compatible Labels for Third Harmonic Generation Microscopy. *Phys. Chem. Chem. Phys.* **2012**, *14*, 10653−10661.
(16) Bartalucci, G.; Coppin, J.; Fisher, S.; Hall, G.; Helliwell, J. R.; Helliwell, M.; Liaaen-Jensen, S. Unravelling the Chemical Basis of the Bathochromic Shift in the Lobster Carapace; New Crystal Structures of Unbound Astaxanthin, Canthaxanthin and Zeaxanthin. *Acta Crystallogr. B* **2007**, *63*, 328−337.
(17) Simpson, G. J.; Perry, J. M.; Moad, A. J.; Wampler, R. D. Uncoupled Oscillator Model for Interpreting Second Harmonic Generation Measurements of Oriented Chiral Systems. *Chem. Phys. Lett.* **2004**, *399*, 26−32.
(18) Perry, J. M.; Moad, A. J.; Begue, N. J.; Wampler, R. D.; Simpson, G. J. Electronic and Vibrational Second-Order Nonlinear Optical Properties of Protein Secondary Structural Motifs. *J. Phys. Chem. B* **2005**, *109*, 20009−20026.
(19) Gualtieri, E. J.; Haupert, L. M.; Simpson, G. J. Interpreting Nonlinear Optics of Biopolymer Assemblies: Finding a Hook. *Chem. Phys. Lett.* **2008**, *465*, 167−174.
(20) Wanapun, D.; Wampler, R. D.; Begue, N. J.; Simpson, G. J. Polarization-Dependent Two-Photon Absorption for the Determination of Protein Secondary Structure: A Theoretical Study. *Chem. Phys. Lett.* **2008**, *455*, 6−12.
(21) Davis, R. P.; Moad, A. J.; Goeken, G. S.; Wampler, R. D.; Simpson, G. J. Selection Rules and Symmetry Relations for Four-Wave Mixing Measurements of Uniaxial Assemblies. *J. Phys. Chem. B* **2008**, *112*, 5834−5848.
(22) Moad, A. J.; Simpson, G. J. Self-Consistent Approach for Simplifying the Molecular Interpretation of Nonlinear Optical and Multiphoton Phenomena. *J. Phys. Chem. A* **2005**, *109*, 1316−1323.
(23) Prakashan Korambath, H. A. K. Frequency-Dependent Polarizabilities and Hyperpolarizabilities of Polyenes. *ACS Symp. Ser.* **1996**, 133−144.
(24) Van Gisbergen, S. J. A.; Snijders, J. G.; Baerends, E. J. Calculating Frequency-Dependent Hyperpolarizabilities Using Time-Dependent Density Functional Theory. *J. Chem. Phys.* **1998**, *109*, 10644.
(25) Kestur, U. S.; Wanapun, D.; Toth, S. J.; Wegiel, L. A.; Simpson, G. J.; Taylor, L. S. Nonlinear Optical Imaging for Sensitive Detection of Crystals in Bulk Amorphous Powders. *J. Pharm. Sci.* **2012**, *101*, 4201−4213.
(26) Muir, R. D.; Kissick, D. J.; Simpson, G. J. Statistical Connection of Binomial Photon Counting and Photon Averaging in High Dynamic Range Beam-Scanning Microscopy. *Opt. Express* **2012**, *20*, 10406−10415.
(27) Toth, S. J.; Madden, J. T.; Taylor, L. S.; Marsac, P.; Simpson, G. J. Selective Imaging of Active Pharmaceutical Ingredients in Powdered Blends with Common Excipients Utilizing Two-Photon Excited Ultraviolet-Fluorescence and Ultraviolet-Second Order Nonlinear Optical Imaging of Chiral Crystals. *Anal. Chem.* **2012**, *84*, 5869−5875.
(28) Kissick, D. J.; Muir, R. D.; Sullivan, S. Z.; Oglesbee, R. A.; Simpson, G. J. Real-Time Dynamic Range and Signal to Noise Enhancement in Beam-Scanning Microscopy by Integration of Sensor Characteristics, Data Acquisition Hardware, and Statistical Methods. In *Proc. SPIE*, 8657, Computational Imaging XI; Bouman, C. A., Pollak, I., Wolfe, P. J., Eds.; **2013**; p 86570E.
(29) Haupert, L. M.; Simpson, G. J. Chirality in Nonlinear Optics. *Annu. Rev. Phys. Chem.* **2009**, *60*, 345−365.
(30) Franz, A. W.; Rominger, F.; Müller, T. J. J. Synthesis and Electronic Properties of Sterically Demanding *N*-Arylphenothiazines and Unexpected Buchwald−Hartwig Aminations. *J. Org. Chem.* **2008**, *73*, 1795−1802.
(31) Hall, V. J.; Simpson, G. J. Direct Observation of Transient Ostwald Crystallization Ordering from Racemic Serine Solutions. *J. Am. Chem. Soc.* **2010**, *132*, 13598−13599.
(32) Chowdhury, A. U.; Dettmar, C. M.; Sullivan, S. Z.; Zhang, S.; Jacobs, K. T.; Kissick, D. J.; Maltais, T.; Hedderich, H. G.; Bishop, P. A.; Simpson, G. J. Kinetic Trapping of Metastable Amino Acid Polymorphs. *J. Am. Chem. Soc.* **2014**, *136*, 2404−2412.
(33) Giron, D.; Goldbronn, C.; Mutz, M.; Pfeffer, S.; Piechon, P.; Schwab, P. Solid State Characterizations of Pharmaceutical Hydrates. *J. Therm. Anal. Calorim.* **2002**, *68*, 453−465.